Chemistry–A European Journal
Research Article
doi.org/10.1002/chem.202202020
Chemistry Europe
European Chemical Societies Publishing
www.chemeurj.org

Using Macrocyclic G-Quadruplex Ligands to Decipher the Interactions Between Small Molecules and G-Quadruplex DNA

Måns Andréasson,[a] Naresh Bhuma,[a] Nils Pemberton,[b] and Erik Chorell*[a]

Abstract: This study aims to deepen the knowledge of the current state of rational G4-ligand design through the design and synthesis of a novel set of compounds based on indoles, quinolines, and benzofurans and their comparisons with well-known G4-ligands. This resulted in novel synthetic methods and G4-ligands that bind and stabilize G4 DNA with high selectivity. Furthermore, the study corroborates previous studies on the design of G4-ligands and adds deeper explanations to why a) macrocycles offer advantages in terms of G4-binding and -selectivity, b) molecular pre-organization is of key importance in the development of strong novel binders, c) an electron-deficient aromatic core is essential to engage in strong arene-arene interactions with the G4-surface, and d) aliphatic amines can strengthen interactions indirectly through changing the arene electrostatic nature of the compound. Finally, fundamental physicochemical properties of selected G4-binders are evaluated, underscoring the complexity of aligning the properties required for efficient G4 binding and stabilization with feasible pharmacokinetic properties.

Introduction

It is widely known that purine-rich regions of DNA and RNA can form secondary structures called G-quadruplexes (G4). These structures will form by the self-stacking of guanine base complexes called G-quartets. G-quartets are square planar arrangements assembled when 3 or 4 guanine bases form internal Hoogsteen hydrogen bonds, each guanine bonded to two other guanines. The G-quartets, and the G4 structure itself, are further stabilized by cation coordination through the carbonyl oxygens on each guanine.[1] G4 structures can display a wide variety of different topologies, such as parallel, antiparallel, and hybrid arrangements. The type of topology depends on the nature of the base sequence, G4-loop (nucleotides connecting the guanines) composition and length, strand orientation, and the type of cation coordinated by the G-quartets, which all correlate to the energetic properties of the G4.[1,2] Several G4s have considerable thermodynamic stability, even higher than double-stranded DNA, and exhibit rapid folding kinetics.[3,4] The formation of G4 DNA requires disruption of the helical arrangement, and these structures are therefore believed to form during processes such as replication, transcription, or negative supercoiling of the nucleic acid strands.[5]

Guanine-rich regions that can form G-quadruplexes display a non-random distribution across the human genome with an abundance in promotor regions, transcriptional regulators, and at the telomeric ends of DNA.[6,7] In fact, more than 40% of all human promotor regions contain at least one G4 motif.[8] They are also more common in oncogenes, have been found to help regulate telomeric maintenance, and play a role in the development of diseases such as neurodegenerative disorders and different types of cancers.[9,10] In addition, there is a 90% occurrence rate of potential G4-forming sequences at the DNA replication origins, which together with their known thermodynamic stability and rapid folding kinetics, suggest that G4s can play a central role in the regulation of DNA replication.[11,12]

G4s can affect protein expression and modulate cell proliferation[13] and a well-known example of a G4-regulated oncogene is *c-MYC*.[14] The *c-MYC* gene is associated with key functions such as cell cycle progression or cell proliferation and is upregulated in 70% of all human cancers.[15] The expression of *c-MYC* is foremost regulated by the gene promoter region (NHEIII) containing the guanine-rich sequence Pu27.[16] The predominant G4 structure in Pu27 is an intramolecular-parallel structure that is generally represented by the mutated sequences Pu22 and Pu24T.[17–19] Ligand-induced stabilisation of the G4 in this sequence has been shown to prevent the transcription of c-*MYC*,[20] and this approach is thus considered a novel therapeutic strategy for the treatment of cancer that circumvents direct interactions with the MYC protein.[21]

Another example of G4s associated with oncogene regulation is *c-KIT*, where dysregulation has been reported in the

[a] *M. Andréasson, Dr. N. Bhuma, Dr. E. Chorell*
Department of Chemistry
Umeå University
90187 Umeå (Sweden)
E-mail: erik.chorell@umu.se
[b] *Dr. N. Pemberton*
AstraZeneca
Pepparedsleden 1
431 50 Mölndal Gothenburg
(Sweden)

Supporting information for this article is available on the WWW under https://doi.org/10.1002/chem.202202020

development of several types of cancers and is the main cause of gastrointestinal cancer.[22] A correlation between the stabilization of these G4 structures and the downregulation of *c-KIT* gene expression has been shown.[23]

Furthermore, it has also been shown that the stabilization of G4s can be a way of targeting diseases related to immunoallergic or autoimmune conditions by the reduction of immunoglobulin secretion and inhibiting class-switch recombination.[24]

The link between G4 structures and both central biological processes and human diseases has spurred the development of a vast collection of ligands with abilities to bind and stabilize G4 structures over the last two decades. The common characteristics of these compounds are often some types of positively charged groups and a heterocyclic aromatic core system, as exemplified by compounds **1–3** in Figure 1. These attributes allow the ligands to effectively stack and bind to the exposed G-quartets that constitute the main G4 binding surface. Reports that describe the rational and stepwise developments of such compounds towards potent and selective G4-binders with more drug-like properties are limited beyond the statement that a flat aromatic core is necessary to engage in hydrophobic " π-π stacking" (arene-arene) interactions with the G4-surface and that charged amines can interact with the DNA phosphate backbone.[25–28] These general statements only give limited assistance in the design of new G4 ligands. A deeper level of knowledge to better understand how to rationalise the ligand design and the chemical attributes of novel G4 ligands in terms of what properties make them potent and selective stabilisers of G4s would, therefore, be a valuable addition to the field of medicinal chemistry.[14,29]

To overcome some of the challenges associated with targeting G4 DNA, macrocyclic compounds can offer a beneficial starting point in terms of ligand design.[30] Macrocycles have been shown to enable design of compounds with good oral pharmacokinetic (PK) properties when operating in the challenging chemical space termed "beyond rule of 5".[31] In other words, they allow for properties such as a molecular weight $>$500 Da, the number of rotatable bonds $>$10, a polar surface area (PSA) $>$140 Å^2, and still retain a good bioavailability in contrary to classical drug-like molecules.[32] The reason for this is often attributed to intramolecular interactions within the macrocycle, e.g., the ability to shield polar groups in a hydrophobic environment or vice versa. In this way, the macrocycle can adjust its molecular shape, and thus its properties, depending on the local chemical environment. It is also recognized that macrocycles can interact and bind selectively to flat and undistinguished binding sites with high affinity.[33,34] This is an important property in the design of G4 ligands considering the flat and rather unspecific binding surface on the exposed G-quartets of G4 structures.

In our previous work, we have shown that macrocyclization can indeed be a powerful tool to generate compounds that strongly bind and stabilise G4 structures while still showing complete selectivity towards G4 DNA over double-stranded DNA.[30] Here, we have further explored this approach and used it as an example in combination with well-known ligands to delineate key properties for efficient G4 ligand design. This required significant synthetic method development to several heterocyclic fragments and generated a new macrocyclic series of G4-ligands with different macrocyclic sizes, molecular architectures, and electronic properties. The novel macrocycles were evaluated for their G4-binding, -stabilization, and -selectivity using orthogonal assays and selected compounds were profiled in key physicochemical assays to determine solubility, LogD, and permeability. This revealed highly efficient and selective macrocycles but also large differences between the analogues. Computational studies comparing both the novel macrocycles and well-known G4 ligands were thus performed, which identified key aspects for rational design of G4-ligands. This information can now be used to drive the development of next-generation G4 ligands with improved properties.

Results and Discussion

Molecular design

Our previous study showed that macrocycle **4** has excellent abilities to selectively bind and stabilize G4 DNA structures by interacting with the exposed G-quartets.[30] To investigate the conformational preference of **4**, we performed a conformational search of **4** in Maestro[35] using the OPLS3e[36] force field as implemented in MacroModel.[37] The Mixed Torsional/Low-Mode sampling (MTLMOD) method was used, and maximum itera-

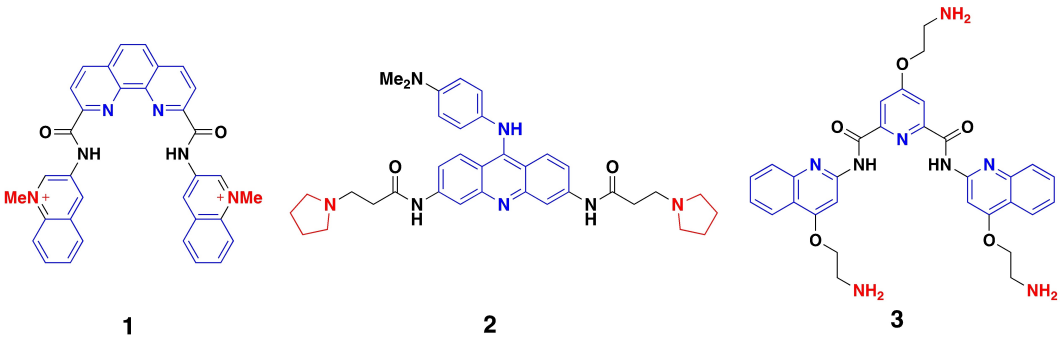

Figure 1. Examples of some well-known scaffolds for G4-stabilising compounds and their important characteristics. Phen-DC3 (**1**), BRACO (**2**), and Pyridostatin (**3**).

tions set to 5 000, the number of steps to 15 000, and RMSD cut-off to 0.5 Å.[38] This showed that the lowest energy populated conformations of **4** exist exclusively in a twisted and distorted shape, imposed by the V-shaped bis-indole scaffold, where the quinolines form intramolecular interactions (Figure 2a). This twisted macrocyclic geometry and the number of aromatic systems is excessive and should intuitively result in a non-optimal structure for interacting with the flat G4-surface. Therefore, the bis-indole scaffold was proposed to be replaced by a tryptamine scaffold (highlighted in magenta) to remove one aromatic system and simultaneously adjust the macrocyclic size and conformation (Figure 2c top).

Starting from the new tryptamine scaffold, we also wanted to replace the indole with a simpler xylene di-amine (highlighted in purple) to explore if the indole plays an essential role in the binding interactions or if its main impact is linked to the macrocyclic molecular architecture and conformation.

Arene-arene interactions are non-covalent interactions that are essential for drug-target binding and recognition, in particular for G4 DNA-binding.[39] We will here avoid the term "π-π stacking" since this often leads to the misconception that a π-orbital overlap is involved in the interactions, which is not the case. Arene-arene interactions for parallel-displaced and face-to-face complexes are foremost composed of two major physical components; dispersion and electrostatic interactions.[40,41] For dispersion, the favorable interaction arises from a temporary induced dipole moment in the aromatic systems, and either electron-rich or -deficient substituents on the arenes in the molecule that bind should be beneficial for binding.[40] For the electrostatic forces, substituents on the ring systems induce a permanent dipole, in contrast to the temporary induced dipole moment in dispersion, that affects the electron distribution in the molecule. Both electron-rich and -deficient arenes in the molecule that binds can result in more favorable electrostatic binding interactions. However, either electron-rich or -deficient are usually the most energetically favourable, and this depends heavily on the electronic nature of the other arene partner.[40–42] Electrostatic potential (ESP) maps are frequently used to display the electron distribution (mapped on the electron iso-surface) of aromatic rings and are powerful tools, especially in combination with assay data, when evaluating how the electronic properties of the arenes impact the arene-arene interactions.[40–43] The arene-arene interactions between heterocyclic aromatic systems are usually less geometrically constrained (the orientation of the interaction arenes) and this is especially true if there is a large difference in polarization between the interacting arenes. In such cases, even the face-to-face (stacked) interaction is more common, which is otherwise generally more disfavoured.[43]

These interactions are central in binding the exposed flat G-quartet that constitute the main binding surface of G4 DNA, and we thus aimed to explore how exchanging the perma-

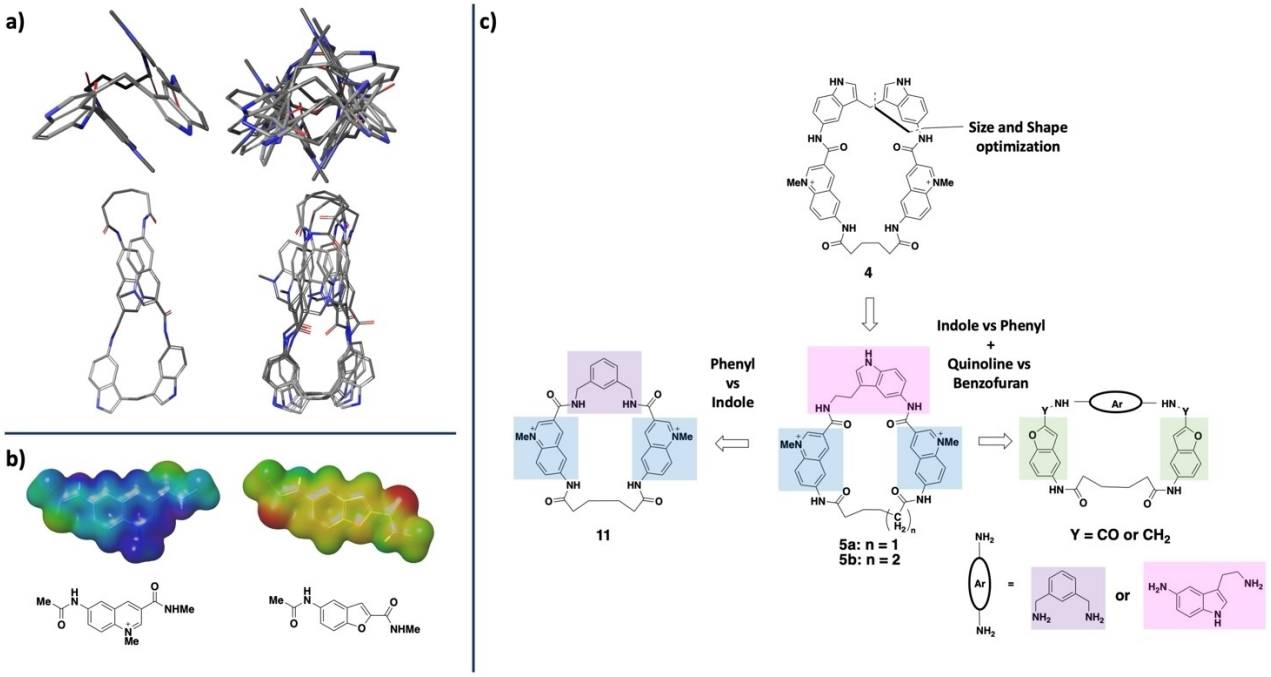

Figure 2. a) Left: The V-shaped bis-indole scaffold present in **4** (side and top view) forces the entire macrocyclic structure into a distorted twisted shape, not optimal for interacting with the planar G4-surface (represented by the populated lowest energy conformation of **4** generated in Maestro[35] using the OPLS3e[36] force field as implemented in MacroModel[37]. a) Right: Superimposed image representative of the lowest energy populated states of **4**. b) Calculation of the ESP for the two fragments (methylated quinoline and benzofuran) was done in the Maestro software.[32] The B3LYP-D3[45] level of theory with the 6-31G** basis set as implemented in Jaguar[46] was used to calculate the geometry optimization and ESP maps for the fragments. The ESP map is shown with an ISO-value of 0.005 and an energy span of −40–160 kcal/mol. The color span represents different energy levels going from red (lowest negative) to blue (highest positive). c) top: Exchange of the bis-indole scaffold to a tryptamine scaffold could optimise the macrocyclic size and geometry for efficient binding to the G4-surface. c) bottom: Summary of the novel macrocyclic compounds and their respective structural features included in this study. The structural motifs are colour coded according to their respective names in the text.

nently charged bis-quinoline (highlighted in blue) core scaffold for a different heteroaromatic core would affect the G4-binding. A benzofuran (highlighted in green) scaffold was chosen as a substitute for the quinoline scaffold. The benzofuran system was selected since it previously has been reported in a type of G4-ligand[44] and because it here represents an electron-rich aromatic system in contrast to the very electron-deficient nature of the methylated bis-quinoline system, as clearly shown on the ESP maps in Figure 2(b). The ESP maps were generated using density functional theory (DFT) geometry optimisations. The calculations were performed on the B3LYP-D3[45] level of theory with the 6-31G** basis set as implemented in Jaguar.[46]

To further advance the study, the difference between *amide* (neutral) or *amine* (positively charged at physiological pH) connectivity for the benzofuran core system was also included. This would show if the cationic charges alone are important for the strong interactions with the guanines on the G4-surface through arene-cation interactions,[47] or if the electronic property of the aromatic core is the main determining factor for strong binding through arene-arene interactions. To investigate the value of macrocyclization, all non-macrocyclic analogues were also included in the study design. The target compounds are summarised in Figure 2(c bottom).

Synthesis

To first address the goal of reducing the size and optimize the shape of the original macrocyclic design (**4**), the tryptamine scaffold **7** was synthesized from 5-nitroindole via electrophilic aromatic substitution with oxalyl chloride followed by quenching with ammonia to afford **6** in 91% yield. A simultaneous reduction of the nitro and oxalyl group with $LiAlH_4$ subsequently afforded compound **7** in lower yields of 24%. We tried to optimise the yield of **7** by formylation on C-3 of 5-nitroindole with the Vilsmeier-reagent and subsequent condensation with nitromethane, followed by global reduction with $LiAlH_4$, but no major improvement in the yield was obtained. The macrocyclization between **8a/b** and **7** was next performed in a dilute DMF solution with chloro-*N*,*N*,*N*′,*N*′-tetramethylformamidinium hexafluorophosphate (TCFH)/N-methylimidazole as coupling reagents and the slow addition of **7** to afford macrocycles **9a/b** in the yields of 25% and 22%, respectively. The methylation of the quinolines using methyl iodide afforded the target macrocycles **5a/b** in moderate to high yields without the need for further purification.

The synthesis of xylene di-amine macrocycle **10** was explored using di-acid **8a** with different coupling reagents (TCFH/N-methylimidazole, (3-Hydroxy-3*H*-1,2,3-triazolo[4,5-*b*]pyridinato-*O*)tri-1-pyrrolidinyl-phosphorus hexafluorophosphate (PyAOP)/N-methylmorpholine, or 1-propanephosphonic anhydride (T3P)/N-methylmorpholine) and finally, (1-Cyano-2-ethoxy-2-oxoethylidenaminooxy)dimethylamino-morpholino-carbenium hexafluorophosphate (COMU®)[48] proved to be the superior alternative, providing a satisfying yield of 61%. Subsequent methylation afforded the target macrocycle **11** in 88% yield (Scheme 1).

We first envisioned diol **16** as a suitable molecular scaffold for obtaining the benzofuran macrocycles (Scheme 2). The aliphatic versions (**20a/b**) via chlorination followed by nucleo-

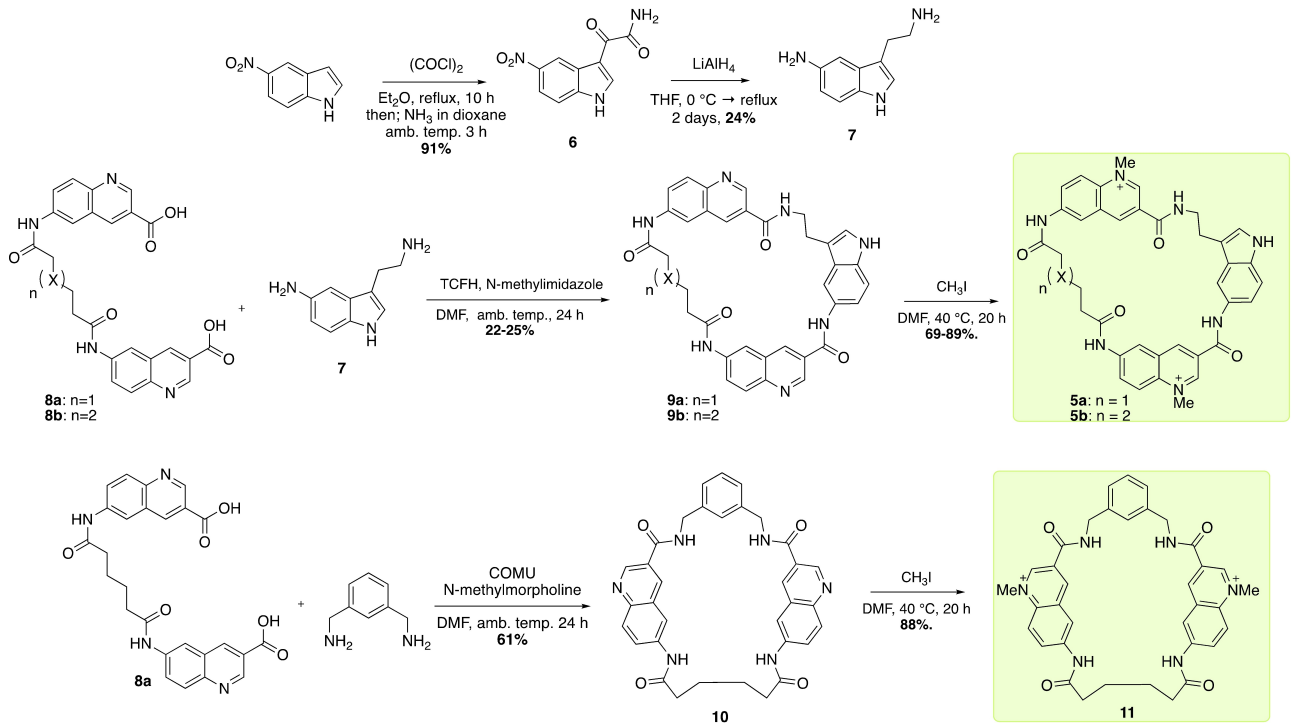

Scheme 1. Synthesis of macrocycles **5a/5b** and **11**.

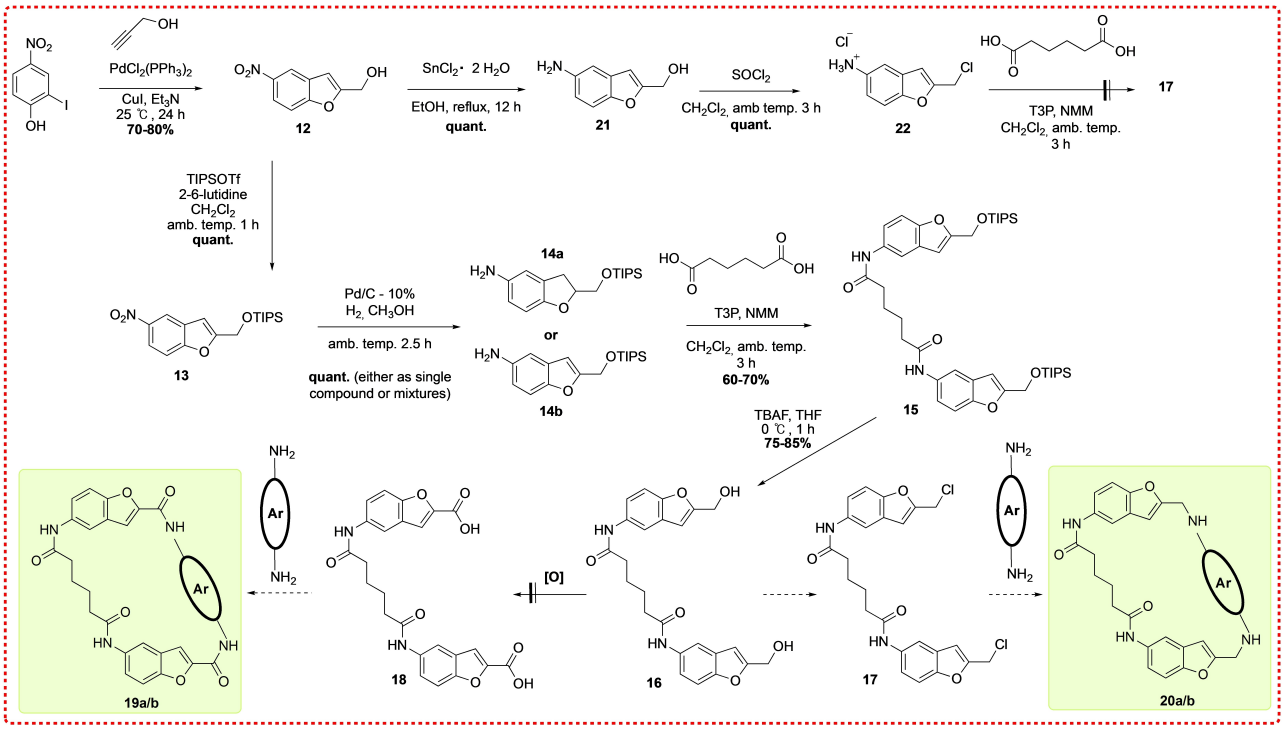

Scheme 2. Initial synthetic plan for the construction of the macrocyclic benzofuran compounds.

philic displacement, and the amide versions (**19a/b**) via oxidation and subsequent amide coupling. Thus, benzofuran alcohol **12** was synthesised from 2-iodo-4-nitrophenol and propargyl alcohol through a Pd-catalyzed cross-coupling/cyclization reaction, providing yields between 70–80%. The bromophenol could also be used, however, giving lower yields and the need for harsher conditions. The alcohol was then quantitatively protected (to avoid unwanted reactions in the upcoming amide coupling) using triisopropylsilyl triflate (TIPSOTf)/2,6-lutidine in CH_2Cl_2 to give compound **13** in quantitative yield. Subsequent reduction of the nitro group proved to be very challenging, often giving mixtures or sometimes complete conversion to the over-reduced compound **14a**. Pt/C with cyclohexadiene in methanol accomplished the nitro reduction to **14b** selectively using microwave irradiation in quantitative yields.[49] This method, however, only worked on a smaller scale (< 50 mg) and was therefore abandoned. After attempts with other reduction conditions, we finally settled with the material of **14b** that we could obtain from the initial conditions (Pd/C), despite the outcome being highly unpredictable. Next, the double amide coupling using two equivalents of **14b** and adipic acid in the presence of T3P (propylphosphonic anhydride) and N-methylmorpholine to give **15** in 60%–70% yield. Deprotection with TBAF gave the desired diol **16** in 75%–85% yields. Next, we pursued the oxidation of the diol **16** to di-acid **18** via a stepwise oxidation using Dess-Martin periodinane (DMP) or 2-iodoxybenzoic acid (IBX). Unfortunately, these attempts were unfruitful leaving diol **16** unreacted. The bottlenecks created by the challenges in the selective formation of **14b** over **14a** and the unsuccessful oxidation of **16** lead to a redesign of the synthesis. We first explored if we could still use **12** to access the aliphatic amine benzofuran macrocycles. Amino-alcohol **21** was successfully obtained from **12** in quantitative yields using $SnCl_2$ in ethanol (the silyl group in **13** was incompatible with these conditions). Subsequent conversion of the alcohol **21** to the chloride **22** with thionyl chloride gave quantitative yields and **22** could be used without further purification. However, efforts to convert **22** into di-chloride **17** were unsuccessful and an unidentified by-product was formed instead, possibly from a polymerisation of **22**. This could be attributed to the incompatible nature of a nucleophile/electrophile combination in the same molecule. The initial synthetic efforts are summarised in Scheme 2.

After revising the pitfalls of the initial synthetic plan, benzofuran ester **23** was a compelling choice as starting material for mainly two reasons (Scheme 3). First, we hypothesized that the electron-withdrawing ester on the furan ring would prevent the unwanted reduction of the furan ring experienced during the hydrogenation of the nitro group (**13** to **14**, Scheme 2). Secondly, the ester is an ideal starting point for the conversion to either an acid or alcohol for further transformation to the amide and amine linkages outlined in the design (Figure 2). Thus, nitro benzofuran (**23**) was reduced using standard Pd/C hydrogenation conditions to afford **24** in quantitative yields without any observable problem of reduction of the furan ring. Subsequent double amide bond formation between **24** and adipic acid using T3P/N-methylmorpholine gave the di-ester **25** in 79% yield. Hydrolysis of the di-ester **25** afforded the di-acid **18** in 90% yield.

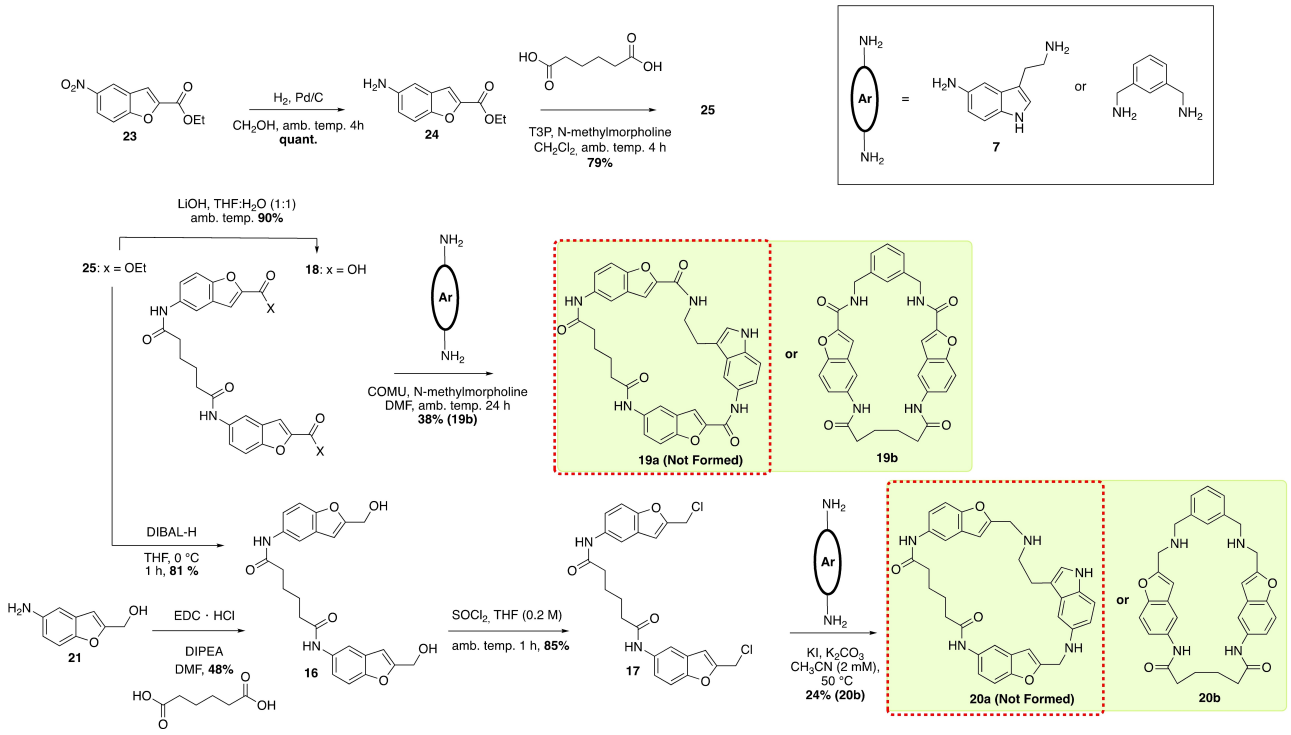

Scheme 3. Total synthetic scheme for the macrocycles **19b** and **20b**.

Correspondingly, diol **16** was obtained in 81% by the treatment of **25** with DIBAL-H in THF at 0 °C for 1 h.

As an alternative method, the amino alcohol (**21**, Schemes 2 and 3) could also be coupled directly with adipic acid to generate **16** in the presence of N-(3-Dimethylaminopropyl)-N′-ethylcarbodiimide hydrochloride (EDC)/diisopropylethylamine (DIPEA), albeit in lower yields of 48%. The diol **16** could next be transformed into **17** in the presence of $SOCl_2$ in THF (0.2 M) in 85% yield. The reason for using a 0.2 M concentration in the chlorination step was that a reduction in the yield and the formation of side products were observed at lower concentrations. It's worth to mention that both **17** and **18** were obtained from **23** without the need for any column purification. Macrocyclizations were next explored using the key intermediates **17** and **18** together with xylene di-amine and **7**. The xylene di-amine was first reacted with di-acid **18** using dilute conditions with COMU/N-methylmorpholine in the double amide macrocyclization coupling, which successfully gave the target macrocycle **19b** in 38% yield. The xylene di-amine was next reacted with the double chloromethyl derivative **17**. This reaction was first attempted in the presence of potassium carbonate in a diluted THF solution at ambient temperature. However, with these conditions, only the unreacted starting materials (xylene di-amine and **17**) were recovered. To thwart this, we heated the reaction to 50 °C and/or added a catalytic amount of potassium iodide. The combination of heating and addition of potassium iodide gave conversion to the macrocycle **20b** albeit very slowly, and after 5 days of stirring, the major species were still the starting materials. This could be improved by exchange of THF for acetonitrile. Hence, the use of potassium iodide and potassium carbonate in a dilute acetonitrile solution at 50 °C gave the desired double amine macrocycle **20b** in 24% yield, with a reaction time of 3 days. Unfortunately, the tryptamine did not give the corresponding macrocycles despite extensive screening with several coupling reagents (T3P (propylphosphonic anhydride)/N-methylmorpholine, EDC/DIPEA, PyAOP/N-methylmorpholine, 1-[[Bis(dimethylamino)methylene]-1*H*-1,2,3-triazolo[4,5-*b*]pyridinium 3-oxid hexafluorophosphate (HATU)/DIPEA, TCFH/N-methylimidazole).

The non-macrocyclic analogues **26** and **27** were synthesised via a double amide coupling between quinoline acid **34** and the di-amines used for the macrocycles (tryptamine **7** or the xylene di-amine). Tryptamine **7** was coupled with **34** using the COMU/N-methylmorpholine conditions to afford **35** in 69% yield whereas the xylene di-amine was coupled using the T3P/N-methylmorpholine conditions to afford **36** in 68% yield. Subsequent methylation of each compound in the presence of methyl iodide in DMF at 40 °C afforded **26** and **27** in 66% and 69% respectively. Compound **28** was obtained in 68% yield from a double amide coupling between the benzofuran acid **30** and xylene di-amine by using T3P/N-methylmorpholine. Finally, to obtain compound **29**, benzofuran acid **30** was reduced to alcohol **31** in the presence of $LiAlH_4$ in 68% yield. The alcohol **31** was then converted to the chloride **32** with the Vilsmeier reagent in a 95% yield. **32** was next reacted with xylene di-amine in the presence of potassium carbonate and potassium iodide in acetonitrile at 40 °C to afford **29** in 41% yield (Scheme 4).

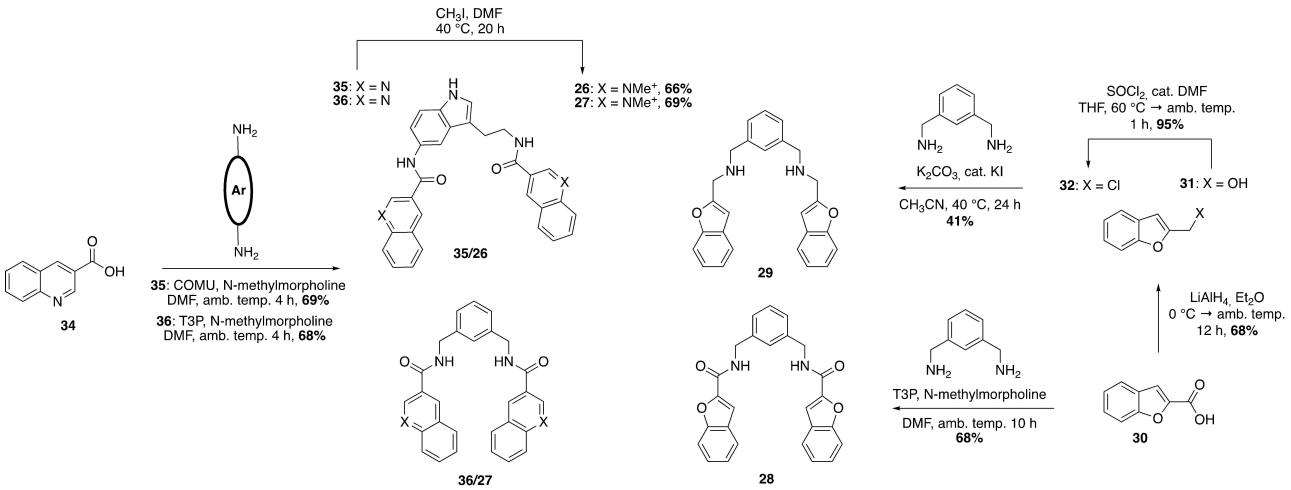

Scheme 4. Synthetic scheme for all the non-macrocyclic analogues (**26**, **27**, **28**, and **29**).

The synthesised set of novel macrocyclic compounds and their corresponding non-macrocyclic analogues are summarised in Figure 3. This set of compounds is well suited to answer the questions regarding the properties of G4-binders that we set out to explore, despite the setback of not obtaining the tryptamine-benzofuran macrocycles. In addition, we chose to include macrocycle **10** as a direct comparison between the permanently charged quinolines (**11**) and the neutral quinoline core (**10**), the latter having a similar ESP map (Figure S12) as the benzofuran (Figure 2c). Hence, all compounds were next evaluated to correlate these structural and electronic modifications to G4-binding, -stabilisation, and -selectivity.

FRET screening assay

To evaluate if the synthesised macrocyclic compounds and their corresponding non-macrocyclic analogues could interact with G4 DNA, we first used a fluorescence resonance energy transfer (FRET) assay with the labelled *c-MYC* G4 DNA structure Pu24T (Table S1). We used this assay to record the $\triangle T_m$ (difference in melting temperature) of the G4 DNA alone and in the presence of all the synthesised compounds (**5a**/**b**, **10**, **11**, **19b**, **20b**, and **26–29**) and reference compound **4**[30] to assess their abilities to bind and stabilise the G4 structure at different concentrations (Figures 4a and S1).

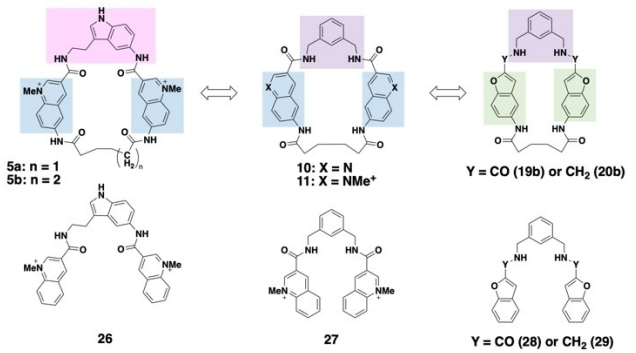

Figure 3. A summary of the successfully synthesized compounds.

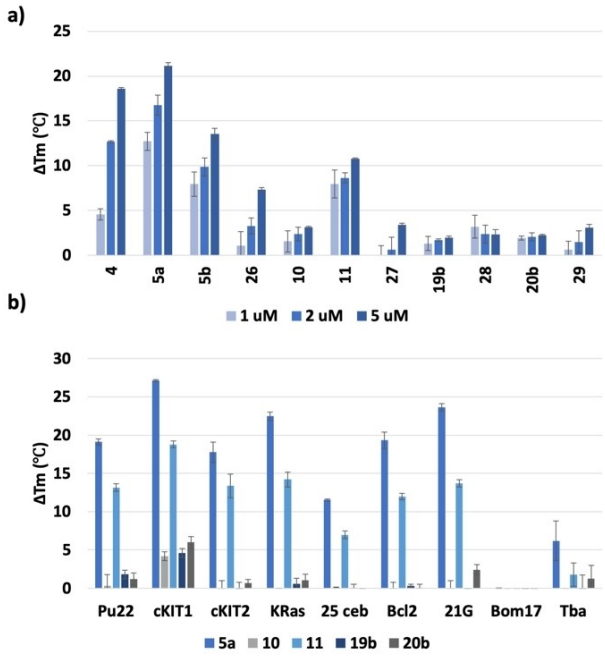

Figure 4. a) The FRET melting assay with the synthesised compounds at 1, 2, and 5 μM concentrations for Pu24T (0.2 μM), showing the ability of the compounds to stabilise the G4 structure. b) The FRET melting assay with **5a**, **10**, **11**, **19b**, and **20b** at 2 μM concentrations for several G4 DNA structures (0.2 μM), showing the ability of the compounds to stabilise the different G4 DNA structures. Pu22 (*c-MYC* promoter); cKIT1, cKIT2 (*c-KIT* promoter); KRas (*K-RAS* gene) and 25 ceb (human minisatellite) are parallel G4 forming sequences. Bcl2 (*BCL-2* promoter) and 21G (human telomere) are hybrid G4 forming sequences. Bom17 (*Bombyx* telomere) and Tba (thrombin binding aptamer) are antiparallel G4 forming sequences. Error bars correspond to SD of at least three independent experiments.

This showed that the replacement of the bis-indole in **4** for the tryptamine scaffold in **5a** resulted in a clear improvement in the thermal stabilisation of Pu24T, especially in the lower concentrations (1 or 2 μM). This supports our theory that removal of one indole system, thereby fine-tuning the macrocyclic structure and fit on the G4-surface, can be an effective way to optimise ligand binding. Interestingly, an evident drop in stabilisation is seen with a single carbon chain extension of the macrocycle, as in **5b**, indicating that the optimal G4-binding interactions are sensitive to the molecular geometry and the pre-organisation of the G4-ligand. This is further corroborated by the additional large decrease in stabilisation observed for the corresponding non-macrocyclic analogue **26**, which also highlights the value of macrocyclization to achieve the correct geometry and pre-organisation for efficient G4 DNA binding and stabilisation.

The stabilisation seen for **11**, where 5-amino-tryptamine (**7**) has been replaced with the xylene di-amine scaffold, is decreased compared to that of the parent tryptamine macrocycle **5a**. This is likely related to how the change from tryptamine (**7**) to the slightly shorter and more flexible xylene di-amine confines the overall macrocyclic structures in conformations that are less favourable for binding the G4-surface. Indeed, when comparing the xylene di-amine-based macrocycle **11** with the one-carbon extended tryptamine-based macrocycle **5b**, their G4-stabilisation are very similar. Comparing the xylene di-amine based macrocycle **11** with its non-macrocyclic analogue **27** once again underscores the striking value of macrocyclization to achieve optimal binding interactions, likely through a better molecular geometry and pre-organisation.

The introduction of an electron-rich heterocycle such as the benzofuran core system in **19b** almost completely abolish all G4-stabilizing abilities. Therefore, having an electron-rich neutral aromatic core system seems detrimental to the interactions with the G4-surface. In fact, removal of the N-methyl groups on the quinolines as in **10** (non-methylated version of **11**), and thus the permanent charges, cause the same loss of G4-binding and stabilisation ability. However, the charge alone cannot be attributed to this because the introduction of a cation in the benzofuran macrocycle via the aliphatic amine connectivity (**20b**) cannot rescue the loss in G4-stabilization, and it remains on the same low level as the neutral amide in **19b**. Thus, protonated cations on the G4-surface do not appear to contribute to any favourable interactions with the guanines via simple arene-cation interactions. These results all point in the direction that electron-deficient aromatic core systems are essential for achieving strong binding interactions. It has previously been indicated in the literature that electron-withdrawing groups or atoms in G4-ligands can be favourable for binding,[25] in agreement with what we observe here. However, it would be ambiguous to base G4-ligand design only on the introduction on electron-withdrawing groups/atoms since this does not always correlate to an electron-deficient ESP map. Therefore, the utilisation of computational tools should serve as more reliable tools for the basis of novel G4-ligand design. These vital interactions between the electron-deficient ligands and the presumed electron-rich guanines on the G4-surface can likely occur through both edge-to-edge and face-to-face arene-arene interactions, putting less geometrical constraints on the ligands for achieving strong binding. It is clear that even minor changes in the compound design can have detrimental effects on the G4-stabilisation ability, as exemplified by both the one-carbon extension of the linker between the quinolines (as in **5a** to **5b**) and by the replacement of the 5-amino tryptamine (**7**) with a xylene diamine (as in **5a** to **11**).

To confirm that the trends observed for the compounds are not just limited to one G4 structure, we screened five of the macrocycles (**5a**, **10**, **11**, **19b**, and **20b**) with several different G4 DNA structures (Table S1). This shows the same internal trend observed for Pu24T, with the 5-amino tryptamine-based macrocycle **5a** as the most efficient stabiliser in all cases, closely followed by the xylene di-amine macrocycle **11**, thus again showing the small difference between replacing these two central fragments. Both these macrocycles show a clear selectivity towards parallel and hybrid G4 structures with a preference for the oncogenic *c-MYC*, *c-KIT*, *KRAS*, *BCL-2* as well as the telomeric 21G G4 structure with $\triangle T_m$ values above 20 °C at 2 μM and a lower stabilization of the parallel 25 ceb (human minisatellite) and antiparallel Bom17 (telomeric) and Tba (Thrombin binding aptamer) G4 structures. The xylene di-amine macrocycles with the benzofuran core (**19b** and **20b**) showed similarly low G4-stabilisation with no internal difference related to the amide vs. amine linkage, which reinforces that protonated cations cannot rescue the weak G4-interactions from the electron-rich benzofuran system. However, both the benzofuran macrocycles (**19b** and **20b**) displayed an increased stabilisation specifically of the *cKIT1* G4 structure with a $\triangle T_m$ of up to 5 °C at 2 μM concentrations (Figures 4b and S2). Overall, this indicates that even though the structural changes investigated have a detrimental effect on the compounds' ability to bind and stabilise G4 DNA structures, it does not have a strong effect on the compounds' ability to discriminate between different G4 topologies. This is logical considering that the compounds are optimised to efficiently bind the core G4-surface, which is identical between G4 structures, whereas their abilities to discriminate between G4s mainly is governed by how sterically accessible the G4-surface is to the molecule that binds and, perhaps, the possibility for additional interactions. In this respect, it would seem that the G4-surfaces of the antiparallel G4s (Bom17 and Tba) are completely or relatively inaccessible to the macrocycles.

We next used circular dichroism (CD) to ensure that the most efficient macrocycles (**5a** or **11**) do not alter the G4-structure upon binding. No change in topology could be observed upon the addition of **5a** or **11** to Pu24T G4 DNA, thereby confirming that the macrocycles do not alter the G4 structure upon binding (Figure S4).

Binding Affinities

To assess how G4-stabilization correlates with G4 DNA-binding, we next performed binding affinity studies for selected macrocycles (**5a**, **11**, **19b**, and **20b**) with the *c-MYC* and *c-KIT* G4

structures (Pu24T, Pu22, and cKIT2). Despite **19b** and **20b** being close to inactive in the FRET assay, we decided to include them in the binding assays since we cannot exclude that the compounds bind G4 DNA without having a high impact on the thermal stability. A fluorescence intercalator displacement (FID) assay was first employed to estimate K_d-values for the ligands. In this assay, the ability of the compound to displace the G4-binder thiazole orange (TO) from the G4 complex by competing for binding is measured in the form of a decrease in fluorescence emission (Figures S5, S6 and S8).

The estimated binding affinities for **5a** and **11** correlate well with the trend from the FRET assay; the 5-amino tryptamine macrocycle **5a** show slightly stronger binding affinity with estimated K_d-values ranging from 0.2–0.6 μM for the different G4 DNA structures, and the xylene di-amine macrocycle **11** display estimated K_d-values ranging from 0.3–1.1 μM (Table 1). This difference is again likely attributed to the better pre-organization in **5a**, imposing the macrocycle in a more optimal ground-state geometry for binding the G-quartet. Furthermore, the improved binding of **5a** compared to **4**,[30] were encouraging and in agreement with the data from the FRET assay. The stabilizing properties of **19b** and **20b** were in agreement with the FID assay, and even at eight equivalents of the macrocycles in relation to, no K_d-values could be obtained for the benzofuran macrocycles (Table 1, Figure S7) for Pu24T (Pu22 and cKIT2 were therefore not tested). This is again in complete agreement with our theory that an electron-deficient aromatic core system is essential for the molecules to engage in strong arene-arene binding interactions with the guanines of the G4-surface.

To further investigate the macrocycles' K_d-values to the G4 DNA structures, we utilised a fluorescence quenching assay with 5'Cy5-labelled G4 DNA sequences Pu24T, Pu22, and cKIT2 (Table S1) by using Microscale Thermophoresis (MST). In this assay, a quenching in fluorescence occurs if the compound binds to the G4 structure, and quenching of the fluorescence emission can then be plotted against compound concentration (Figure S9).

Macrocycle **5a** again proved to be the superior binder with K_d-values in the nanomolar range (90–130 nM). The mono-indole macrocycle **5a** is a better binder to all three G4 structures evaluated as compared to the starting bis-indole macrocycle **4**[27] (Table 2), which again validates the design hypothesis for the transition from **4** to **5** (Figure 2).[30] The same trend in binding affinity is observed between **5a** and **11**, with **11** having a preference for the two *c-MYC* G4 structures over the *c-KIT* G4. However, a more significant difference between **5a** and **11** is observed in this assay, with **11** displaying K_d-values in the micromolar range (3.1–5.1 μM). Finally, the benzofuran macrocycles (**19b** and **20b**) were evaluated for their ability to bind the Pu24T G4 structure. However, even at 100 μM of the added macrocycle, no decrease in fluorescence signal could be observed, which thus confirms the inability of the benzofuran macrocycles (**19b** and **20b**) to bind this G4 structure (Figure S10).

Table 1. Estimated K_d-values from the FID assay of different G4 DNA (Pu24T, Pu22, and cKIT2) at 0.25 μM for different concentrations of the macrocycles. N. D. = Not possible to determine.

macrocycle	*est* K_d [μM] for Pu24T	*est* K_d (μM) for Pu22	*est* K_d (μM) for cKIT2
4	0.99 ± 0.02	0.23 ± 0.01	0.44 ± 0.02
5a	0.60 ± 0.11	0.19 ± 0.03	0.13 ± 0.04
11	1.12 ± 0.01	0.27 ± 0.03	0.57 ± 0.01
19b	*N. D.*	–	–
20b	*N. D.*	–	–

Table 2. Measured K_d-values from the fluorescence quenching assay of different G4 DNA (Pu24T, Pu22, and cKIT2) at 0.25 nM for different concentrations of the macrocycles. *N. D.* = Not possible to determine.

macrocycle	K_d [μM] for Pu24T	K_d (μM) for Pu22	K_d (μM) for cKIT2
4	0.77 ± 0.09	0.90 ± 0.11	0.31 ± 0.03
5a	0.13 ± 0.01	0.09 ± 0.01	0.13 ± 0.01
11	3.27 ± 0.13	3.45 ± 0.38	5.11 ± 0.96
19b	*N. D.*	–	–
20b	*N. D.*	–	–

Selectivity Towards G4 DNA

We next performed the FRET melting assay with the fluorescently labelled dsDNA to investigate if the macrocyclic architecture of **5a** and **11** result in selective G4 DNA-stabilisation without affecting dsDNA, (Table S1). The assay was performed in an analogous way to the first FRET assay but using the change in $\triangle T_m$ of dsDNA as readout at different concentrations of **5a** and **11** (Figure S3a). This showed that none of the macrocycles had any impact on the stability of dsDNA at the tested concentrations (1, 2, 5 μM). To further challenge these results, we performed a FRET-based competition assay. Here, we measured the $\triangle T_m$ of Pu24T (0.2 μM) in the presence of **5a** or **11** (2 μM) with increasing equivalents (0, 15, 50, and 100 equivalents) of added dsDNA (ds26) (Figure S3b). Both macrocycles showed complete retention in their abilities to stabilize Pu24T, even at 100 equivalents of added dsDNA.

Compound Calculations

To better understand and rationalise the assay data that we have obtained for the compounds, we performed molecular mechanics (MM) calculations. Conformational searches for the macrocycles (**5a**/**b**, **11**, **19b**, and **20b**) were performed using Maestro[35] to find the lowest energy populated states for each macrocycle. In the case of the 5-amino-tryptamine macrocycle **5a**, a large part of the lowest energy populated conformations is represented by a relatively flat compound geometry, which enables all three of the aromatic systems to bind the G4-surface simultaneously (Figures 5a, b and S11). However, the conformational preference for the one-

carbon extended macrocycle **5b** is very different, favouring a more twisted compound geometry where only two out of the three aromatic systems are in the same plane (Figures 5a, b and S12). This will likely result in a considerable entropic penalty

Research Article
doi.org/10.1002/chem.202202020
Chemistry Europe
European Chemical Societies Publishing

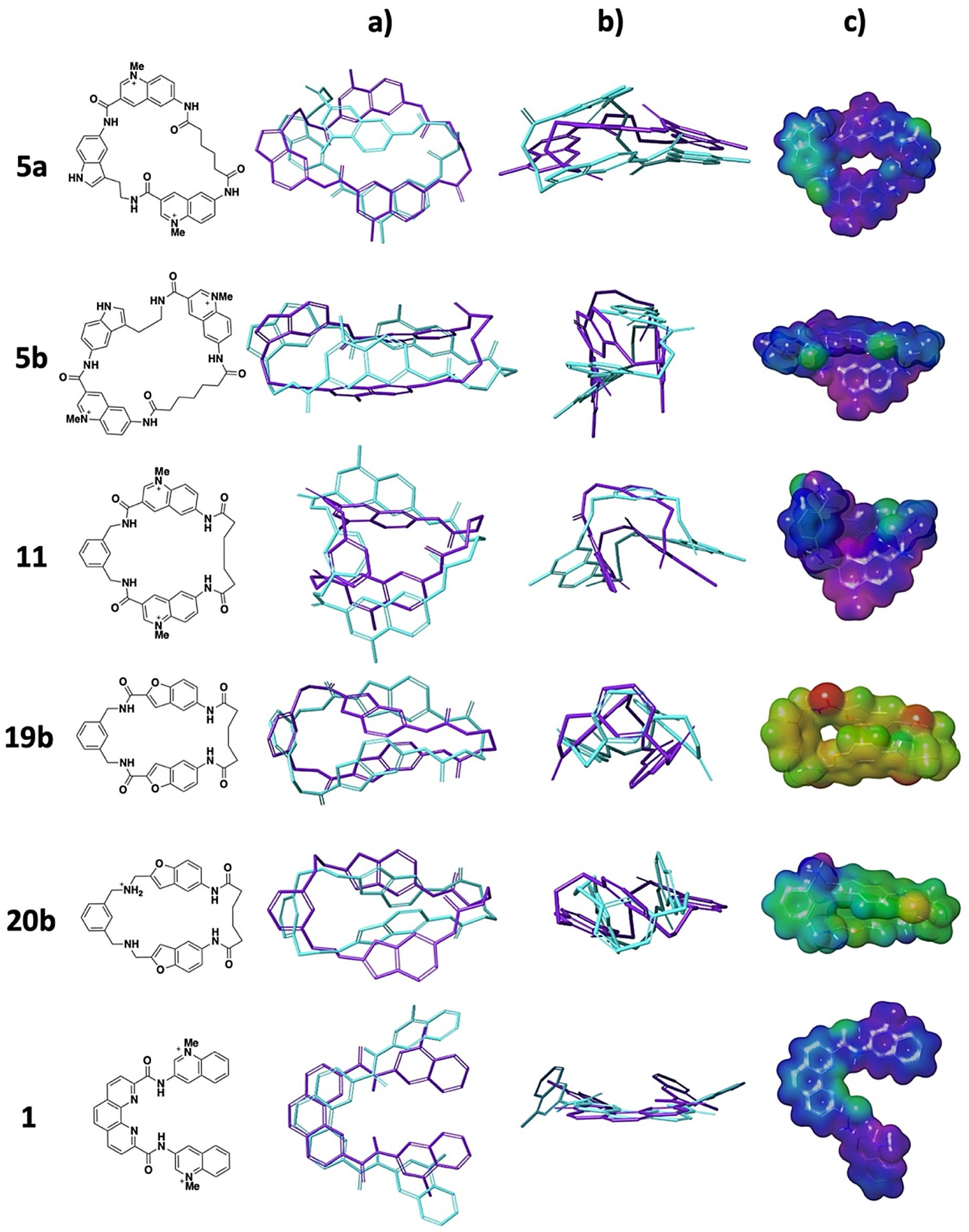

Figure 5. a) Superimposed image representative of the lowest energy populated states for each compound viewed from the top. b) Superimposed image representative of the lowest energy populated states for each compound viewed from the side. c) Optimized geometry of the compound showing the ESP map with an ISO-value of 0.005 and an energy span of 40– 160 kcal/mol. The colour span represents different energy levels going from red (lowest negative) to purple (highest positive).

during the binding event for **5b** compared to **5a**, which could explain the difference in their abilities to bind and stabilise the G4 DNA structures despite only varying by one carbon atom in the macrocyclic linkage. The conformational preference for the xylene di-amine macrocycle **11** is similar to the one-carbon extended 5-amino-tryptamine macrocycle **5b**, with only two out of three aromatic systems having the correct geometry to bind simultaneously (Figures 5a, b and S15). This can explain why **5b** and **11** have similar stabilizing properties. Overall, this shows how important it is to consider the conformational preferences of the target molecules when developing new G4-binding compounds since minor structural differences can result in significant differences in G4-binding and -stabilisation. For the benzofuran macrocycles **19b** and **20b** (Figures 5a, b, S16 and S17), the geometry is non-optimal, with the compounds having a non-planar conformation in accordance with **5b** and **11**. This alone would, however, not explain the compounds' inability to bind G4 DNA. Complementary to our macrocycles, we performed the same MM calculations for the known G4-binders Phen-DC3 (**1**), BRACO (**2**), and Pyridostatin (**3**) (Figure 1). The conformational preference of Phen-DC3 (**1**) is highly pre-organized and relatively flat, with all the aromatic system in an almost planar geometry (Figures 5a, b and S18). The binding event of Phen-DC3 (**1**) to the G4-surface should consequently be associated with a small entropic penalty.

A similar case is seen for BRACO (**2**) and Pyridostatin (**3**) (Figures S20, S22 and S24).

Geometry optimisations and ESP calculations for the macrocycles (**5a**/**b**, **11**, **19b**, and **20b**) were next conducted using Maestro[35] on the low-energy conformations. We used the B3LYP–D3[45] level of theory with the 6–31G** basis set as implemented in Jaguar[46] to explore the electronic properties of each macrocycle. From this, the ESP map of **5a** shows that the methylated quinolines drastically affect the electronics of the entire macrocycle, giving an overall electron-deficient species (Figure 5c). This is again in line with that an electron-deficient compound is crucial to engage in strong binding interactions with the G4-surface. As expected, we saw the same trend for **5b** (Figure 5c) and **11** (Figure 5c), both showing electron-deficient ESP maps spread out over the entire macrocycle. We performed analogues calculations for compound **10** (the non-methylated version of **11**), and while the conformational preference between **11** and **10** is similar (Figure S13, S15), the ESP map of **10** display a far more electron-rich species (Figure S14). To validate these calculations, the ESP map for the well-known G4-ligand Phen-DC3 (**1**, Figure 1) was calculated. This shows the same type of electron-deficient nature as in **5a**/**b** and **11** (Figures 5c and S19), which thus further emphasises the importance of this property for strong binding interactions. The ESP maps of the benzofuran macrocycles are significantly different as well, and **19b**, with amide linkage, shows an overall electron-rich macrocycle (Figure 5c), similar to non-methylated quinoline **10**. Based on the assay data and compound calculations, the G4-surface must therefore be an electron-rich aromatic system, and consequently, the compound that binds must have an electron-deficient nature for the arene-arene interactions to be favorable and result in a strong binding event. This reasoning would explain why **19b** has displayed no ability to bind any of the G4 structures. To clarify, we are not stating that benzofurans are unavoidably poor G4-binders, but instead highlight the importance to tune the electronic properties of the aromatic system correctly. The ESP map for the benzofuran macrocycle with an amine linkage (**20b**) is more electron-deficient relative to **19b**, but much less so in relation to the other macrocycles (Figure 5c). The protonated amine in the benzofuran macrocycle **20b** makes this derivative more electron-deficient. However, based on our assay data, this effect, in addition to the poor conformational preference of the compound, is not prominent enough to make **20b** a strong G4 binder. Furthermore, aliphatic amines on known G4-binding compounds are commonly placed as flexible extended tails, facing away from the G4 binding surface.[28] To investigate this, we calculated the ESP maps for the known G4-binders Pyridostatin[28] (**3**) and BRACO[28] (**2**) that entails such aliphatic amine side chains (Figures 1 and S21, S23, S25). For Pyridostatin (**3**), we chose to include both the bis- and tris-protonated forms of the compound. In the bis-protonated form, we protonated only one of the symmetrical amines and the unsymmetrical amine that is attached to the pyridine ring. The ESP map for Pyridostatin (**3**) is also electron-deficient and thus in line with being an efficient G4-ligand. The electron-deficient system is in this case caused by the withdrawing effects of the protonated amines, and a similar effect is seen for BRACO (**2**). Fine-tuning of the aromatic core of G4-ligands to achieve optimal binding through arene-arene interactions will require additional studies, for example, to explore the synergistic energetic effects of both dispersion and electrostatics on the binding interactions.

It is usually attributed in the literature that the protonated amines in G4-ligands enable strong electrostatic binding interactions with the charged phosphate backbone of the DNA.[28] However, it is well-known to medicinal chemists that ligand-target interactions between ions (salt-bridges) in solvent exposed areas contribute little or nothing to the overall binding energy due to the high desolvation costs of the charged interacting species.[50,51] It therefore seem unlikely that these interactions themselves are in part responsible for the strong binding to G4s, even though they probably occur. This supports the notion that charged amines likely contribute more to the binding energy by tuning the electrostatic properties of the aromatic systems that bind, rather than through specific electrostatic interactions with the phosphate backbone. We, therefore, conclude that aliphatic amines should be placed outside the central aromatic core to partake in favorable solvation interactions during the binding event and simultaneously making the compound more electron-deficient, which thereby enhance arene-arene interactions.

Physicochemical Profiling

Finally, we measured key physicochemical properties for selected compounds (Table 3). Aqueous solubility for all the synthesised macrocycles was low, with slightly higher values obtained for **20b**, likely because of the partially protonated

Table 3. Physicochamical Profiling. [a] Distribution coefficient between 1-octanol and aqueous phosphate buffer at pH 7.4 [c] Intrinsic permeability measured in Caco2 cells incubated at pH = 6.5 with a cocktail of inhibitors of common transporters. N.V. = No Value, N.T. = Not Tested.

Compound	log $D_{7.4}$[a]	Aq. Solubility pH 7.4 [μM]	Caco2 P_{app} A–B Papp [10^{-6} cm/s][b]
Phen-DC3 (1)	−0.2	107	N.T.
5a	−0.9	N.V.	1.4
10	2.3	3	0.4
11	< −1	< 2	0.1
19b	2.0	< 2	N.T.
20b	3.3	22	N.T.
26	−0.2	340	N.T.
27	−0.6	230	N.T.
28	N.V.	3	N.T.
29	4.6	28	N.T.

aliphatic amine. The open-chain analogues **26** and **27** both showed higher solubility, which could be attributed to the greater conformational freedom relative to the macrocycles. We also chose to include **10**, the non-methylated version of **11**, and the known G4-binder Phen-DC3 (**1**). **10** had roughly the same solubility as **11**, while Phen-DC3 (**1**), similar to the previously mentioned open-chain analogues, had good solubility. All the charged methylated compounds had negative log D-values, while matched pair analogue **10** was considerably more lipophilic with a log*D* of 2.3, being more similar to the benzofurans. We then measured intrinsic Caco2 permeability for selected analogues, good permeability is key to achieving high in vivo absorption and bioavailability for oral compounds and is also an indication of how well the compounds can permeate a cell membrane. Compound **11**, which has a permanent charge and a negative log*D* value, showed low permeability in the Caco2 assay. The matched pair analogue **10** that does not carry any permanent charges has about four times higher permeability than **11**. This highlights the value of G4 ligands without permanent charges, as the charged analogues are very hydrophilic and will be challenging to optimise further to obtain compounds with high permeability and thus suitable for oral dosing. Encouragingly, the new potent macrocycle **5a** show slightly higher permeability and one can speculate that this compound might be able to permeate cell membranes and can potentially be further evaluated in cellular assays.

Conclusion

In this work, we have developed synthetic methods for several heterocyclic fragments and combined them into a series of novel macrocyclic and non-macrocyclic compounds with diverse properties, starting from macrocycle **4** as a basis for our compound design. The generated macrocycles and their non-macrocyclic counterparts were evaluated using orthogonal assays to measure G4-stabilization, -binding, and -selectivity. Selected compounds were also profiled in physicochemical assays to determine solubility, Log*D*, and permeability. This disclosed large differences between the analogues and several important details regarding this compound class and how it can be optimised. Essentially, the combination of these studies with computational analyses that also included well-known G4-ligands as reference compounds revealed key aspects for the design of G4-ligands that confirm previous studies and expand the current state of knowledge; A) macrocyclization can offer a powerful starting point for G4-ligand design by imposing a pre-organisation within the molecule, making the molecular geometry more closely matched to the geometry of the optimal binding conformation. This is further demonstrated by how the careful modification and fine-tuning of the macrocyclic size and geometry can generate very potent compounds, as exemplified by going from compound **4** to **5a**. Furthermore, a macrocyclic structure renders the compounds completely selective for G4 DNA over dsDNA. B) Ligand conformation is of key importance to investigate and to assure that a satisfying molecular conformation for the targeted compounds is fulfilled, MM calculations should be conducted as a part of the compound design. This is encouraged to avoid the pitfalls of compounds that might look appealing in two dimensions but that will exist in twisted geometries and poor conformational preferences to bind the G4-surface. C) Electron-deficient aromatic systems are essential for the compounds to engage in strong arene-arene interactions with the G4 binding surface, exemplified by the electron-deficient methylated quinolines. Thus, for novel G4-ligands, it is crucial to design the compounds such that the quantum mechanics (QM) calculations of the targeted compounds display an electron-deficient ESP map, especially for the aromatic core systems that bind the G4-surface. The total synergistic energetic impact of arene-arene interactions from both dispersion and electrostatic forces on binding and stabilisation of G4s, however, remains to be seen. D) Protonated amines can serve as powerful means to change the electrostatic nature of the compound while maintaining favourable solvation interactions during the binding event. This is exemplified by Pyridostatin (**3**), BRACO (**2**), and **20b**; however, we believe that the amine should not be positioned directly at the centre of the G4-surface since classical arene-cation interactions appear to not improve the binding. In this context, N-methylation of for example quinolines to form permanent charges can strongly improve G4-binding and this can be related to tuning the electrostatic properties of the molecules into very electron-deficient species, making them strong G4-binders. However, the negative log*D*-values and the poor passive permeability that such species often impose render them unsuitable as motifs for further developments towards biological applications.

We hope that these detailed suggestions combined with previously published G4 ligand design aspects can serve as starting points or guidelines for rational G4-ligand design that could benefit other researchers and ultimately catalyse the development of these types of compounds towards therapeutic interventions and thus explore the potential of G4 DNA as therapeutic targets.

Experimental Section

Folding of G4 structures for FRET study: Synthetic labelled oligonucleotides for FRET study were purchased from Eurofins Genomics. Stock solutions were prepared in water at 100 μM concentration. The sequences used are listed in Supporting Table S1. All the oligonucleotides except Pu22 were prefolded in 10 mM lithium cacodylate buffer (pH 7.4), with 10 mM KCl and 90 mM LiCl by heating for 5 min at 95 °C and then quick cooling on ice. Pu22 was folded in 10 mM lithium cacodylate buffer (pH 7.4), with 2 mM KCl and 98 mM LiCl.

FRET melting assay: The fluorescence resonance energy transfer (FRET) occurs between two dyes (5′-FAM as donor and 3′-TAMRA as acceptor) linked at both extremities of a DNA oligonucleotide. When the oligonucleotides are folded into G4 structures, the donor and acceptor are in proximity, which results in an energy transfer from the donor to the acceptor. This process can be detected by a reduction in the fluorescence emission of the donor. Fluorescence emission of the donor is recovered when the temperature increment triggers the thermal denaturation of the G4 structure. The experiments were performed in a Bio-rad CFX96 real-time PCR device at temperatures from 10 to 95 °C at 1.5 °C/m heating rate using a 492-nm excitation wavelength and a 516-nm detection wavelength in 96-well plates. Each condition was tested in duplicate, and analysis of the data was carried out by using Excel and Origin 8 software. In each well, 0.2 μM of labelled oligonucleotide was heated in the presence or absence of the ligand (and with or without the competitor dsDNA) at the specified concentrations. Emission of 5′-FAM was normalized between 0 and 1, and the melting temperature (T_m) is defined as the temperature at which 50% of the G4 structures are denatured (the temperature when the normalized emission was 0.5). The stabilization ($\triangle T_m$) is calculated from comparison of T_m of the fluorescently labelled oligonucleotide in the presence or absence of the ligand.

Fluorescence Intercalator Displacement (FID) Experiments: Synthetic oligonucleotides for FID study were purchased from Eurofins Genomics. Stock solutions were prepared in water at 1 mM concentration. The sequences used are listed in Supporting Information Table S1. All the oligonucleotides (0.25 μM) were folded in 10 mM K-phosphate buffer (pH 7.4), with 100 mM KCl by heating for 5 min at 95 °C and then allowed for cooling to room temperature. The experiments were performed at 25 °C on a Jasco FP-6500 spectrofluorometer equipped with a temperature controller. The pre-folded G4-DNA (0.25 μM) was mixed with 0.50 μM Thiazole Orange (TO) and incubated for 2 minutes before the fluorescence spectrum was recorded (λ_{ex} = 501 nm; λ_{em} = 510–650 nm) Then ligands were added to the mixture stepwise with a 2 min equilibration period, and the fluorescence spectra were recorded. The percentage of TO displacement was calculated from the fluorescence intensity (F) at the emission maxima, using the following equation:

$$\textbf{Percentage of TO displacement} = 100 - \left(\frac{F}{F_0} \times 100\right)$$

where, F_0 is the initial fluorescence intensity of TO bound to G4-DNA.

The percentage of TO displacement was plotted as a function of the concentration of added ligands and DC_{50} is determined. The binding constant (K_d) of the ligands were calculated from the following equations using K_a^{To} as $1.55 \times 10^6\ M^{-1}$, $5.01 \times 10^6\ M^{-1}$ and $6 \times 10^6\ M^{-1}$ for Pu24T, Pu22 and c-KIT2 respectively:

$$K_a^{ligand} = \frac{K_a^{TO} \times [TO]}{[ligand]_{50}} \quad K_d^{ligand} = \frac{1}{K_a^{ligand}}$$

Fluorescence-Based Quenching using Micro Scale Thermophoresis (MST): 5′-Cy5 labelled G4 DNAs for this study were purchased from Eurofins Genomics. Stock solutions were prepared in water at 100 μM concentration. The sequences used are listed in Supporting Information Table S1. The G4 DNA sequences were folded in KCl buffer (10 mM phosphate, 100 mM KCl, pH 7.4) by heating at 95 °C for 5 min and then cooling to room temperature. All the experiments were performed in 10 mM phosphate pH 7.4, 100 mM KCl, 0.05% Tween20. The labelled DNA concentration is held constant at 25 nM and ligand concentration is varied from 0.15 nM to 10 μM for 5a or 3.05 nM to 100 μM for 11, 19b, and 20b (fourteen 1:1 dilutions). The samples were loaded into standard MST graded glass capillaries and initial fluorescence intensity of the capillary were measured using Monolith NT.115 (Nano Temper, Germany) with 40% LED power. The change in fluorescence with ligand's concentrations were plotted in Excel and fitted through non-linear equation to obtain the binding constants.

Compound Calculations: The calculations were performed in Maestro[35] v. 11.9.011 for windows-64bit as a part of the Schrödinger package. The conformational searches for the macrocycles were conducted using MacroModel[37] with the OPLS3e[36] force field without solvent using a dielectric constant of 3. The Mixed Torsional/Low-Mode sampling (MTLMOD) was used, and maximum iterations were set to 5 000, number of steps to 15 000, and RMSD cut-off to 0.5 Å.[38] The conformational search for all non-macrocyclic compounds were performed in the same way with the only exception being that the number of steps were set to 10 000. The ESP maps were generated using DFT geometry optimisations. The calculations were performed on the B3LYP-D3[45] level of theory with the 6-31G** basis set as implemented in Jaguar.[46] Only one amine in **20b** was protonated for the calculations since we found it unlikely that both will be protonated at physiological pH when in such proximity to each other.

Acknowledgements

Work in the Chorell lab was supported by the Kempe foundations (SMK-1632) and the Swedish Research Council (VR-NT 2017-05235).

Conflict of Interest

The authors declare no conflict of interest.

Data Availability Statement

The data that support the findings of this study are available in the supplementary material of this article.

Keywords: arene-arene interactions · G-quadruplex DNA · G4-ligand · macrocycle · molecular design

[1] M. Kogut, C. Kleist, J. Czub, *Nucleic Acids Res.* **2016**, *44*, 3020–3030.
[2] A. Bugaut, S. Balasubramanian, *Biochemistry* **2008**, *47*, 689–697.

[3] A. N. Lane, J. B. Chaires, R. D. Gray, J. O. Trent, *Nucleic Acids Res.* **2008**, *36*, 5482–5515.
[4] A. J. Dingley, R. D. Peterson, S. Grzesiek, J. Feigon, *J. Am. Chem. Soc.* **2005**, *127*, 14466–14472.
[5] D. Sun, L. H. Hurley, *J. Med. Chem.* **2009**, *52*, 2863–2874.
[6] N. Maizels, L. T. Gray, *PLoS Genet.* **2013**, *9*, e1003468.
[7] V. S. Chambers, G. Marsico, J. M. Boutell, M. Di Antonio, G. P. Smith, S. Balasubramanian, *Nat. Biotechnol.* **2015**, *33*, 877–881.
[8] J. L. Huppert, S. Balasubramanian, *Nucleic Acids Res.* **2007**, *35*, 406–413.
[9] G. Biffi, D. Tannahill, J. Miller, W. J. Howat, S. Balasubramanian, *PLoS One* **2014**, *9*, e102711.
[10] N. G. Dolinnaya, A. M. Ogloblina, M. G. Yakubovskaya, *Biochemistry* **2016**, *81*, 1602–1649.
[11] N. Maizels, *EMBO Rep.* **2015**, *16*, 910–922.
[12] P. Prorok, M. Artufel, A. Aze, P. Coulombe, I. Peiffer, L. Lacroix, A. Guédin, J.-L. Mergny, J. Damaschke, A. Schepers, C. Cayrou, M.-P. Teulade-Fichou, B. Ballester, M. Méchali, *Nat. Commun.* **2019**, *10*, 3274.
[13] D. Varshney, J. Spiegel, K. Zyner, D. Tannahill, S. Balasubramanian, *Nat. Rev. Mol. Cell Biol.* **2020**, *21*, 459–474.
[14] R. Hänsel-Hertsch, M. Di Antonio, S. Balasubramanian, *Nat. Rev. Mol. Cell Biol.* **2017**, *18*, 279–284.
[15] C. V. Dang, *Cell* **2012**, *149*, 22–35.
[16] J. Seenisamy, S. Bashyam, V. Gokhale, H. Vankayalapati, D. Sun, A. Siddiqui-Jain, N. Streiner, K. Shin-ya, E. White, W. D. Wilson, L. H. Hurley, *J. Am. Chem. Soc.* **2005**, *127*, 2944–2959.
[17] A. Ambrus, D. Chen, J. Dai, R. A. Jones, D. Yang, *Biochemistry* **2005**, *44*, 2048–2058.
[18] N. Deng, L. Wickstrom, P. Cieplak, C. Lin, D. Yang, *J. Phys. Chem. B* **2017**, *121*, 10484–10497.
[19] A. T. Phan, V. Kuryavyi, H. Y. Gaw, D. J. Patel, *Nat. Chem. Biol.* **2005**, *1*, 167–173.
[20] B.-J. Chen, Y.-L. Wu, Y. Tanaka, W. Zhang, *Int. J. Biol. Sci.* **2014**, *10*, 1084–1096.
[21] J. R. Whitfield, M.-E. Beaulieu, L. Soucek, *Front. Cell Dev. Biol.* **2017**, *5*, 10.
[22] Y. Yarden, W. J. Kuang, T. Yang-Feng, L. Coussens, S. Munemitsu, T. J. Dull, E. Chen, J. Schlessinger, U. Francke, A. Ullrich, *EMBO J.* **1987**, *6*, 3341–3351; J. A. Fletcher, B. P. Rubin, *Curr. Opin. Genet. Dev.* **2007**, *17*, 3–7; M. Nannini, G. Biasco, A. Astolfi, M. A. Pantaleo, *J. Med. Genet.* **2013**, *50*, 653–661.
[23] D. Wei, J. Husby, S. Neidle, *Nucleic Acids Res.* **2015**, *43*, 629–644.
[24] Z. Dalloul, P. Chenuet, I. Dalloul, F. Boyer, J.-C. Aldigier, B. Laffleur, Y. El Makhour, B. Ryffel, V. F. J. Quesniaux, D. Togbé, J.-L. Mergny, J. Cook-Moreau, M. Cogné, *J. Allergy Clin. Immunol.* **2018**, *142*, 1352–1355.
[25] A. R. Duarte, E. Cadoni, A. S. Ressurreição, R. Moreira, A. Paulo, *ChemMedChem* **2018**, *13*, 869–893.
[26] S. Asamitsu, T. Bando, H. Sugiyama, *Chem. Eur. J.* **2019**, *25*, 417–430.
[27] A. Ohnmacht, S. Neidle, *Bioorg. Med. Chem. Lett.* **2014**, *24*, 2602–2612.
[28] R. Chaudhuri, S. Bhattacharya, J. Dash, S. Bhattacharya, *J. Med. Chem.* **2021**, *64*, 42–70.
[29] S. Asamitsu, S. Obata, Z. Yu, T. Bando, H. Sugiyama, *Molecules* **2019**, *24*, 429.
[30] R. N. Das, M. Andréasson, R. Kumar, E. Chorell, *Chem. Sci.* **2020**, *11*, 10529–10537.
[31] C. A. Lipinski, F. Lombardo, B. W. Dominy, P. J. Feeney, *Adv. Drug Delivery Rev.* **1997**, *23*, 3–25.
[32] B. C. Doak, J. Kihlberg, *Expert Opin. Drug Discovery* **2017**, *12*, 115–119.
[33] B. Over, P. Matsson, C. Tyrchan, P. Artursson, B. C. Doak, M. A. Foley, C. Hilgendorf, S. E. Johnston, M. D. L. Iv, R. J. Lewis, P. McCarren, G. Muncipinto, U. Norinder, M. W. D. Perry, J. R. Duvall, J. Kihlberg, *Nat. Chem. Biol.* **2016**, *12*, 1065–1074.
[34] B. C. Doak, J. Zheng, D. Dobritzsch, J. Kihlberg, *J. Med. Chem.* **2016**, *59*, 2312–2327.
[35] *Maestro*, version 11.9.011, Schrödinger LLC: New York.
[36] K. Roos, C. Wu, W. Damm, M. Reboul, J. M. Stevenson, C. Lu, M. K. Dahlgren, S. Mondal, W. Chen, L. Wang, R. Abel, R. A. Friesner, E. D. Harder, *J. Chem. Theory Comput.* **2019**, *15*, 1863–1874.
[37] *MacroModel*, version 11.1, Schrödinger LLC: New York.
[38] G. Olanders, H. Alogheli, P. Brandt, A. Karlén, *J. Comput.-Aided Mol. Des.* **2020**, *34*, 231–252.
[39] E. A. Meyer, R. K. Castellano, F. Diederich, *Angew. Chem. Int. Ed.* **2003**, *42*, 1210–1250; *Angew. Chem.* **2003**, *115*, 1244–1287.
[40] M. Watt, L. K. E. Hardebeck, C. C. Kirkpatrick, M. Lewis, *J. Am. Chem. Soc.* **2011**, *133*, 3854–3862.
[41] S. L. Cockroft, J. Perkins, C. Zonta, H. Adams, S. E. Spey, C. M. R. Low, J. G. Vinter, K. R. Lawson, C. J. Urch, C. A. Hunter, *Org. Biomol. Chem.* **2007**, *5*, 1062.
[42] S. E. Wheeler, J. W. G. Bloom, *J. Phys. Chem. A* **2014**, *118*, 6133–6147.
[43] L. M. Salonen, M. Ellermann, F. Diederich, *Angew. Chem. Int. Ed.* **2011**, *50*, 4808–4842; *Angew. Chem.* **2011**, *123*, 4908–4944.
[44] D. R. Calabrese, X. Chen, E. C. Leon, S. M. Gaikwad, Z. Phyo, W. M. Hewitt, S. Alden, T. A. Hilimire, F. He, A. M. Michalowski, J. K. Simmons, L. B. Saunders, S. Zhang, D. Connors, K. J. Walters, B. A. Mock, J. S. Schneekloth, *Nat. Commun.* **2018**, *9*, 4229.
[45] A. D. Becke, *Phys. Rev. A* **1988**, *38*, 3098–3100; C. Lee, W. Yang, R. G. Parr, *Phys. Rev. B* **1988**, *37*, 785–789; S. Grimme, J. Antony, S. Ehrlich, H. Krieg, *J. Chem. Phys.* **2010**, *132*, 154104.
[46] *Jaguar*, version 8.3, Schrödinger LLC: New York.
[47] R. Wintjens, J. Liévin, M. Rooman, E. Buisine, *J. Mol. Biol.* **2000**, *302*, 395–410.
[48] A. El-Faham, F. Albericio, *J. Pept. Sci.* **2010**, *16*, 6–9.
[49] J. F. Quinn, C. E. Bryant, K. C. Golden, B. T. Gregg, *Synfacts* **2010**, *2010*, 492–492.
[50] A. Fischer, M. Smieško, M. Sellner, M. A. Lill, *J. Med. Chem.* **2021**, *64*, 2489–2500.
[51] C. Bissantz, B. Kuhn, M. Stahl, *J. Med. Chem.* **2010**, *53*, 5061–5084.

Manuscript received: June 29, 2022
Accepted manuscript online: August 23, 2022
Version of record online: September 19, 2022